Available online at www.sciencedirect.com
SCIENCE DIRECT®
Journal of Chromatography A, 989 (2003) 165–173
JOURNAL OF CHROMATOGRAPHY A
www.elsevier.com/locate/chroma

Adsorptive membrane chromatography for purification of plasmid DNA

M.A. Teeters, S.E. Conrardy, B.L. Thomas, T.W. Root, E.N. Lightfoot*
Department of Chemical Engineering, University of Wisconsin-Madison, 1415 Engineering Drive, Madison, WI 53706-1691, USA

Abstract

Adsorptive membranes were investigated for the downstream processing of plasmid DNA by quantifying both separation efficiencies and adsorption uptake with the anion-exchange membranes. Separation efficiencies of the 10-ml Mustang-Q were measured using pulses of 6.1-kilo base pair plasmid DNA and lysozyme tracers, and comparing the responses for both conventional and reverse-flow operation. The plasmid exhibited nearly 200 plates/cm, almost as high efficiency as the protein despite the large difference in size. This behavior contrasts strongly with typical behavior for spherical porous particle packings, which predicted large decreases in efficiency with increases in tracer size. Batch adsorption isotherms for the 6.1-kilo base pair plasmid on small sheets of anion-exchange membranes at various ionic strengths showed high capacities for very large biomolecules. The maximum binding capacity for the membrane unit was calculated as 10 mg plasmid/ml, an order of magnitude greater than typical values reported for porous beads.
© 2003 Elsevier Science B.V. All rights reserved.

Keywords: Membranes; Adsorption; Efficiency; Binding capacity; DNA

1. Introduction

Recent advances in gene therapy have increased the need for large-scale production of effective vectors. The latter may be either non-viral (naked and lipid-coated plasmid DNA) or viral (most often adenovirus or retrovirus), and are much larger than the therapeutic proteins their genes encode. While these vectors may commonly be purified in the laboratory using cesium chloride centrifugation or extraction with organic solvents, these bench-scale techniques are difficult to scale up, and they use toxic reagents [1]. Large-scale purifications require scalable methods such as column chromatography [2,3] and tangential flow filtration [4]. In this study we characterize the utility of ion-exchange membranes for chromatographic purification of very large biomolecules by showing both the effect of solute size on membrane efficiencies and plasmid DNA adsorption isotherms at various ionic strengths.

Adsorption measurements of different plasmid DNA [5–7] and a model virus [8] on porous chromatographic media have revealed severe limitations in the capacity for such large biomolecules. In one study, the reported binding capacities of 10 different anion-exchange adsorbents for a 6.9-kilo base pair (kb) plasmid ranged from $\ll 1$ to 5 mg plasmid/ml adsorbent [6]. This is orders of magnitude lower than corresponding capacities for proteins. The largest capacities (~5 mg/ml) occurred in ''superporous'' adsorbents (~650 nm pore sizes). Adsorbents with pore sizes on the order of 100 nm

*Corresponding author. Tel.: +1-608-262-1092; fax: +1-608-262-5434.
E-mail address: enlight@engr.wisc.edu (E.N. Lightfoot).

0021-9673/03/$ – see front matter © 2003 Elsevier Science B.V. All rights reserved.
doi:10.1016/S0021-9673(03)00027-X

had smaller capacities that increased roughly proportionally with reciprocal mean particle radius. This suggests that the plasmid was binding only to the outer surface of the particle, a result also suggested by Ljunglof et al. [7] using confocal microscopy. These results are not surprising, noting the large size of plasmids and viruses (Table 1) relative to typical pore sizes.

Alternative adsorbents, such as micropellicular stationary phases [9], monoliths [10], and adsorptive membranes [11,12], have also been studied for their utility in purification of large biomolecules. Micropellicular adsorbents, specifically 1–5 μm nonporous silica particles, offer both greater outer surface areas for adsorption and increased mass transfer efficiencies compared to the larger particles (15–200 μm) [9]. Pressure drop limitations, however, restrict large-scale applicability, and the surface area for binding is still small. A second class of adsorbents, monoliths, present large convective through-pores that allow high rates of mass transfer at lower pressure drops. Their utility for large biomolecules was demonstrated in a monolithic column with 1.5 μm convective through-pores, as a capacity of 7.9 mg plasmid/ml was measured [10].

Finally, adsorptive membranes [13–15] have been studied for over a decade as an alternative to conventional resin-based chromatography columns. Like monolithic columns, the interactions between dissolved molecules and the active sites on the membrane occur in convective through-pores rather than in stagnant fluid inside the pores of an adsorbent particle. For this reason, the membrane units have the potential to maintain high efficiencies both at high flow-rates and for use with large biomolecules with small diffusivities. This was demonstrated in a 10-ml ion-exchange membrane unit by observing the response to small tracer pulses of AMP (M_r=345), lysozyme (M_r≈14 300), and thyroglobulin (M_r≈650 000) at flow-rates from 10 to 50 ml/min [12]. Intrinsic membrane efficiencies were minimally affected by large increases in flow-rate and solute size. Similarly, the absence of mass transfer limitations in membrane chromatography were observed by Yang et al. [11] in the capture of a small and large protein, α-lactalbumin and thyroglobulin, respectively, as static capacities were equal to the corresponding dynamic capacities.

Accessibility of ion-exchange sites in the large convective pores and the absence of transport limitations make adsorptive membranes an attractive option for the purification of very large biomolecules, including plasmid DNA and viruses. In this paper, we extend our previous work in characterizing membrane efficiencies to include a 6.1-kb plasmid DNA. In addition, plasmid adsorption to strong anion-exchange membranes is quantified and modeled, and the capacity and desorption constants at various ionic strengths are reported.

2. Theory

2.1. Modeling column efficiency

For differential chromatography, solute effluent concentration is frequently approximated by a Gaussian distribution:

$$c(L,t) = \frac{m_0}{A\varepsilon v} \cdot \frac{1}{\sqrt{2\pi\sigma_t^2}} \cdot \exp\left[\frac{-(t-t_r)^2}{2\sigma_t^2}\right] \qquad (1)$$

where c is the concentration of solute exiting a column of length L at time t. Here t_r is the mean residence time of the solute and σ_t is the standard deviation of its distribution in time. Both micro-

Table 1
Molecular sizes and diffusion coefficient order of magnitude of representative biomolecules [24,25]

Biomolecule	Molecular mass	Base pairs	Equivalent sphere diameter (nm)	$\mathcal{D}$ (cm^2/s)
Small molecule	<1000	–	–	10^{-5}
Lysozyme	14 300	–	2.1	10^{-6}
Thyroglobulin	650 000	–	8.5	10^{-7}
Adenovirus	–	–	80	10^{-8}
Plasmid DNA	$3.3\cdot10^6$–$13.2\cdot10^6$	5000–20 000	150–250	10^{-8}–10^{-9}

scopic factors, described below in a one-dimensional model, as well as macroscopic factors, such as non-uniform flow through the column, can contribute to the overall dispersion. It may be seen that a single parameter, σ_t^2/t_r^2, is sufficient to characterize the sharpness of the peak. The inverse of this parameter is conventionally defined as the number of theoretical plates, N, and the efficiency of the packing is described by the height equivalent to a theoretical plate, H, where:

$$N = \frac{t_r^2}{\sigma_t^2} = \frac{L}{H} \tag{2}$$

The most reliable means of determining N or H from experimental data is to recognize that these quantities are given by moments of the effluent concentration distribution:

$$t_r = \frac{\int_{-\infty}^{\infty} ct\,\mathrm{d}t}{\int_{-\infty}^{\infty} c\,\mathrm{d}t} \tag{3}$$

$$\sigma^2 = \frac{\int_{-\infty}^{\infty} c(t-t_r)^2\,\mathrm{d}t}{\int_{-\infty}^{\infty} c\,\mathrm{d}t} \tag{4}$$

We must recognize that the number of plates is only defined for a Gaussian distribution and that approximate methods must be used to deal with non-Gaussian distributions. We extend this definition to non-Gaussian distributions [16,17], using moments in our calculations of apparent plate numbers.

To predict the theoretical plate height of a packed bed in terms of underlying transport and thermodynamic parameters, we will use the model proposed by Athalye et al. [18] as a basic reference. The dispersive mechanisms considered are the mass transfer through a diffusional boundary layer about the particle, intraparticle diffusion to and from the adsorption sites, the finite kinetics of the adsorption/desorption process, and interparticle axial dispersion resulting from axial diffusion and local flow non-uniformities between particles. The model provides a dimensionless plate height, $h = H/d_p$, which is the height of a theoretical plate divided by the average particle diameter, and has the form [18]:

$$h = \frac{2}{\mathrm{Pe}} + \frac{(1-u)^2}{3(1-\epsilon_b)} \cdot (\mathrm{ReSc}) \left[\frac{1}{\mathrm{Nu}_{\mathrm{BL}}} + \frac{m}{\mathrm{Nu}_{\mathrm{IP}}} + \frac{m'}{\mathrm{Da}} \right] \tag{5}$$

In principle, the magnitudes of all broadening mechanisms can be predicted from separately measured properties. It should be noted that these microscopic sources of dispersion occur on a distance scale δ of the order of the particle diameter d_p and that the microscopic dispersion always increases in the direction of flow. We will use this model to compare experimentally measured membrane efficiencies to typical packed bed efficiencies.

2.2. Non-ideal behavior

Not included in the above model are two macroscopic sources of dispersion: macroscopic non-uniform flow in the packing and non-uniform residence time distributions in the inlet and outlet distributors. These tend to occur on a distance scale Δ much greater than the particle diameter d_p. Moreover, flow through a chromatographic column is normally characterized by very low Reynolds numbers:

$$\mathrm{Re} \equiv \frac{\rho v d_p}{\mu} \ll 1 \tag{6}$$

where v is the interstitial velocity, ρ is the fluid density, and μ is the fluid viscosity. Such flows are described by the creeping flow equations of continuity and motion [19]:

$$(\nabla \cdot v) = 0 \tag{7}$$

$$\nabla^2 v = \frac{1}{\mu} \cdot \nabla P \tag{8}$$

These equations are both linear in velocity, and it follows that these flows are reversible as they change sign but not magnitude with the sign of the driving pressure. Flow through porous headers and columns that follows Darcy's law are examples of such reversible flow [20]:

$$\mathbf{v_0} = \mathbf{v}\varepsilon_b = -\frac{\kappa}{\mu} \cdot \nabla P \tag{9}$$

Here ε_b is the void fraction and κ is the permeability of the medium. Reversing the pressure gradient reverses the direction but not the magnitude of the velocity; hence, each fluid element will retrace the path originally made in the opposite direction.

Recall that the microscopic dispersion occurring on a length scale δ is irreversible, that is invariant to changes in the direction of flow, and that fluid motions occurring on a length scale Δ are reversible. This provides the basis of the reverse-flow technique: if the direction of flow is reversed when a small pulse of solute is partway down the column and the solute flows back out the former inlet, any dispersion caused by macroscopic flow variations will be eliminated. The microscopic dispersion, however, is irreversible and independent of the direction of flow, and will continue and be additive as the solute flows up the column. The resulting elution profile will include only irreversible sources of dispersion. This experiment allows one to decouple the effects of microscopic and macroscopic dispersion, and comparison of a reverse-flow dispersion test to a conventional dispersion test allows us to quantify their relative effects [12,21–23].

2.3. Modeling solute retention

The Langmuir isotherm is a simple and ubiquitous model for protein and plasmid [5] adsorption onto ion-exchangers, and will be used in this paper to model the adsorption–desorption equilibrium of plasmid DNA with anion-exchange membranes. Here the rate of plasmid adsorption is given by:

$$\frac{dq}{dt} = k_1 c(q_{max} - q) - k_{-1} q \tag{10}$$

where q is the solid-phase plasmid concentration, c is the liquid-phase plasmid concentration, q_{max} is the maximum solid-phase concentration, or capacity, of the adsorbent, and k_1 and k_{-1} are the forward and reverse rate constants, respectively. At equilibrium, Eq. (10) can be arranged as:

$$q = \frac{q_{max} K_A c}{1 + K_A c} = \frac{q_{max} c}{K_D + c} \tag{11}$$

where $K_D = 1/K_A = k_{-1}/k_1$ is the dissociation constant, equal to the liquid-phase plasmid concentration in equilibrium with $q = q_{max}/2$. Here the isotherm is written using the dissociation rather than the association constant due to the simple interpretation and relevance to capture of plasmids in dilute solutions. All measured adsorption isotherms are fit to Eq. (11).

3. Experimental

3.1. Materials

All chemicals and the protein (lysozyme) used were from Sigma (St. Louis, MO, USA) and buffers were prepared with 18 MΩ water. The mobile phase used for all dispersion tests was a 50 m*M* Tris, 1 m*M* EDTA buffer solution, pH 8.0, with 1 *M* NaCl added. Mustang-Q anion-exchange membranes (Pall, Ann Arbor, MI, USA) were used in three different configurations. Free membrane sheets were cut and used for batch experiments, a six-layer 2.2 cm diameter membrane stack in an Acrodisk (Pall) holder was used in the plasmid purification, and the 10 ml Mustang-Q was used for dispersion tests. Frozen *Escherichia coli* cell paste containing a 6.1-kb plasmid DNA (pCI-luc-kan plasmid, 6103 bp) was obtained from the Waisman Clinical BioManufacturing Facility (Madison, WI, USA).

3.2. Apparatus

The stacked-membrane column analyzed using dispersion tests was a Mustang-Q with a 10 ml nominal bed volume. The Mustang-Q membranes are polyethersulfone (PES) membranes chemically modified to produce a quaternary amine surface. The nominal pore size of the PES membranes is 0.8 μm, and the thickness of each membrane layer is 70–90 μm. The membrane layers are housed in a stainless steel ring with porous frits on each side, and 10 ml Mustang modules are rated to 17 bar. The Mustang module housing was engineered with a design goal of achieving plug flow, consisting of a tapered open gap region above a flat porous frit.

A Waters 2690 separations module and a 2487 dual-wavelength absorbance detector (Milford, MA, USA) were used for all 10 ml Mustang-Q dispersion test experiments. Eluent concentration was monitored by the UV detector used at 260 nm for plasmid

DNA and 280 nm for lysozyme. A Cary UV–Visible spectrophotometer (Palo Alto, CA, USA) was used for concentration measurements in batch experiments at 260 nm. A Beckman Model J2-J20 Centrifuge (Beckman Coulter, Fullerton, CA, USA) was used with both JA10 and JA20 rotors.

3.3. Lysis and plasmid purification

One gram of cell paste (wet mass) was thawed at room temperature for 10 min and resuspended in 10 ml of a 50 m*M* dextrose, 25 m*M* Tris, 10 m*M* EDTA buffer solution, pH 8.0, with 20 μg/ml RNase A (Fisher, Fair Lawn, NJ, USA). The solution was mixed until completely homogeneous before 10 ml of lysis solution [200 m*M* NaOH, 1% (w/v) sodium dodecylsulfate (SDS)] was added. The solution was gently mixed by inversion and allowed to incubate at room temperature for 5 min. Following the cell lysis, 10 ml of a neutralization solution (3 *M* KOAc, 2 *M* HOAc, pH 5.5, chilled to 4 °C) was added and gently mixed by inversion. The resulting solution was incubated on ice for a total time of 30 min, being gently mixed again after 10 min of incubation. The solution was then centrifuged at 22 000 *g* for 30 min at 4 °C. The supernatant was removed, centrifuged for 5 additional min, and filtered through a membrane disk with a 0.2-μm filtration limit. The plasmid in solution was precipitated by adding 0.6 volumes of isopropanol and incubating at room temperature for 1 h. After centrifugation at 10 000 *g* for 30 min at ambient temperature, the pellets were resuspended in a 50 m*M* Tris, 1 m*M* EDTA, pH 8.0 buffer with 500 m*M* NaCl. The plasmid solution was finally loaded by syringe onto the six-layer Mustang-Q membrane Acrodisk, contaminants were washed with 5 ml of 50 m*M* Tris, 1 m*M* EDTA, pH 8.0 buffer with 500 m*M* NaCl, and the plasmid was finally eluted with 1.5 *M* NaCl added to the buffer. Plasmid was again precipitated with isopropanol, centrifuged, and resuspended at the desired salt concentration for batch equilibrium experiments, dispersion tests, or analysis.

Sufficient quantities of 6.1-kb plasmid DNA for batch adsorption experiments and column dispersion tests were purified using the standard alkaline lysis and ion-exchange membrane chromatography as described above. Very gentle mixing of the lysis solution with the cell suspension was necessary to eliminate chromosomal DNA contamination. Contaminant RNA could not be completely removed without the use of RNase. Addition of RNase to the cell suspension was sufficient to digest the RNA into small pieces that did not adsorb to the ion-exchange membrane under plasmid loading conditions.

3.4. Gel electrophoresis

Plasmid DNA as well as chromosomal DNA and RNA contaminants were identified using 0.8% agarose gels, with 0.5 μg/ml ethidium bromide dissolved in solution. The plasmid and a 1-kb DNA step ladder (Promega, Madison, WI, USA) were loaded onto the gel and electrophoresis was carried out at 100 V for 1 h in a TAE running buffer. Samples were visualized and photographed under short-wave length UV light. The purified plasmid was predominantly supercoiled as shown by gel electrophoresis in Fig. 1. At the lowest loading, a faint band of supercoiled plasmid is observed, and it is not until 100 times the lowest loading that the open-circular plasmid band is observed on the gel. Plasmid purity was also confirmed with UV absorbance, where A_{260}/A_{280} equaled 1.8–1.85.

3.5. Restriction digests

Purified and concentrated plasmid fractions were added to the appropriate restriction enzyme buffer with 0.1 mg/ml BSA. The restriction enzymes *Bam*HI and *Hin*dIII (Promega) were separately used,

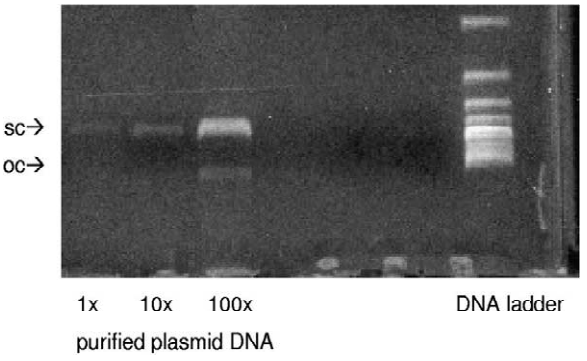

Fig. 1. Agarose gel analysis of supercoiled (sc) and open circular (oc) fractions of purified plasmid DNA at different loadings.

respectively, cutting the plasmid into one linear strand (6.1 kb) and two strands (5.8 and 0.3 kb) for identification in gel electrophoresis. Incubation of the digests occurred overnight at 37 °C prior to loading onto an agarose gel as described above. Comparison of both restriction digests to linear DNA standards on agarose gel electrophoresis confirmed the plasmid was 6.1 kb.

3.6. Dispersion tests

The 10-ml Mustang-Q module was cleaned with five column volumes (5 CVs) of 1 *M* NaOH, regenerated with 5 CVs of 1 *M* NaCl, and equilibrated with 5 CVs of the mobile phase used for all dispersion tests: 50 m*M* Tris, 1 m*M* EDTA, 1 *M* NaCl, pH 8.0. Injections of 50 μl of the plasmid solution (250 μg/ml) and lysozyme solution (10 mg/ml) were made at flow-rates from 1 ml/min to 10 ml/min under high salt conditions (1 *M* NaCl) where they were not retained by the membrane. For the reverse-flow dispersion tests, the direction of flow was reversed at a time equal to one-half the solute residence time of the corresponding forward-flow experiment. Triplicates were made of each run at each flow-rate. The peripheral volume and dispersion were measured by the effluent profiles of corresponding injections in the absence of the column.

3.7. Adsorption isotherms

Free sheets of Mustang-Q anion-exchange membranes were cut into pieces with a cross sectional area of 0.5 or 1 cm^2. The membranes were cleaned in a 1 *M* NaOH solution, regenerated in 1 *M* NaCl, and equilibrated in a solution with the desired salt concentration (100–1000 m*M* NaCl) for the batch experiments. Plasmid solutions were prepared with 100, 400, 500, 600, 700, and 1000 m*M* NaCl in a 50 m*M* Tris, 1 m*M* EDTA buffer, pH 8.0 at concentrations up to 120 μg/ml all in 1.5-ml microcentrifuge tubes. The membrane sheets were subsequently added to the corresponding plasmid solutions. The plasmid solution and membranes were equilibrated on a shaker table at 280 rpm and ambient temperature for 24 h, after which no more adsorption was observed. The equilibrium liquid phase plasmid concentration was measured by absorbance at 260 nm (extinction coefficient = 0.02 $cm^2/\mu g$), and the mass of plasmid bound to the membrane was determined by an overall mass balance. Solid phase plasmid concentrations are reported as μg/cross-sectional membrane sheet area. The batch experiments were done in triplicate for each plasmid loading at each salt concentration.

4. Results and discussion

4.1. Membrane efficiencies

Forward-flow and reverse-flow dispersion tests were run on the 10-ml Mustang-Q using lysozyme and 6.1-kb plasmid DNA tracer spikes. Resulting effluent curve shapes and positions were independent of tracer concentration under the operating conditions described above. Retention volumes were consistent with the interstitial membrane volume, so non-specific interactions that may be occurring between the tracers and the membrane in the high salt conditions are likely to be small. Fig. 2 shows forward-flow and reverse-flow effluent curves of the plasmid DNA at 1 ml/min. The reverse-flow curve is sharper and more symmetrical than the corresponding forward-flow curve, and the difference was ascribed to non-uniform header residence times. This was previously confirmed by numerical simulation

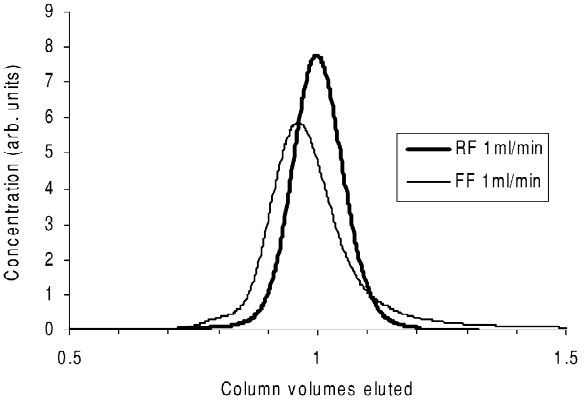

Fig. 2. Comparison of forward-flow and reverse-flow elution profiles from the 10 ml Mustang-Q. Small injections of 6.1-kb plasmid DNA were made under non-retaining conditions at 1 ml/min.

[12]. The reverse-flow elution curves are a measure of lateral diffusional resistance and localized axial dispersion, and show the potential of the stacked membranes in an ideal column. The reverse-flow curve in Fig. 2 gives nearly 200 apparent plates in a membrane stack only 0.97 cm thick. The forward-flow peak indicates actual behavior determined to be 25 apparent plates, showing that macroscopic factors inherently limit performance.

Behavior of a protein and plasmid DNA in the stacked membrane column are compared in Fig. 3, an overlay plot of the reverse-flow curves for lysozyme and plasmid DNA at 5 ml/min. Lysozyme was chosen as a model tracer because it is well characterized, stable, and provides a contrast with the transport properties of the much larger plasmid. The plasmid elution curve has only slightly more dispersion than observed for lysozyme. Membrane efficiencies with plasmid tracers are almost as high as when using protein tracers, despite diffusion coefficients that differ by roughly two orders of magnitude. The insensitivity to solute size and transport properties, even for molecules as large as plasmid DNA, make membranes very attractive for purifying the large gene therapy vectors. In addition, plate numbers for the lysozyme tracer were consistent with previous tests run on the 10-ml Mustang-S [12], indicating the dispersion is independent of the chemistry on the base membrane.

A summary of all experimental data on the 10-ml Mustang-Q and Mustang-S [12] is shown in the modified Van Deemter plot in Fig. 4, where the measured plate heights for both forward- and reverse-flow operation are plotted against percolation velocity divided by solute diffusivity in free solution. No characteristic diameter is included since none exists for membrane stacks. For comparison to the performance of a typical chromatography column, the plot also includes the behavior representative of a solute traveling through a bed packed with 15 μm particles, with plate height predicted by Eq. (5). The intrinsic membrane plate heights determined by the reverse-flow experiments are over an order of magnitude lower than the plate heights predicted for 15 μm particles, and only increase slightly with large increases in scaled velocity. Only modest increases in plate height are noticed when going from the smallest solutes AMP ($M_r = 345$) to the largest thyroglobulin ($M_r \approx 650\,000$) and 6.1-kb plasmid DNA ($M_r \approx 4\,000\,000$). The membrane is not perfectly homogeneous, so we believe the small increases in plate heights with velocity are due to diffusion between regions with local velocity variations. This behavior contrasts strongly with that predicted for conventional granular columns, which shows large increases in plate heights with large increases in scaled velocity. Conventional packings are limited by slow intraparticle diffusion, while

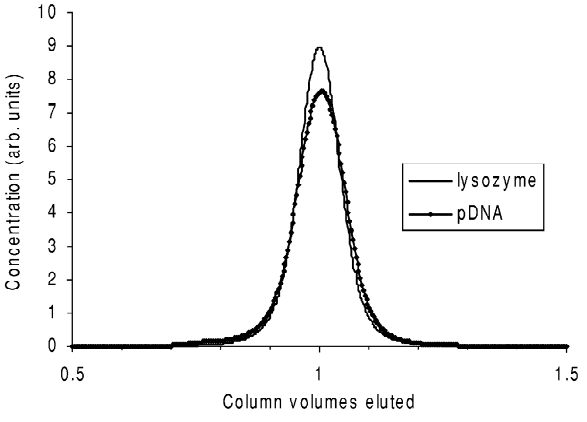

Fig. 3. Comparison of reverse-flow elution profiles from the 10-ml Mustang-Q. Small injections of 6.1-kb plasmid DNA and lysozyme were made under non-retaining conditions at 5 ml/min.

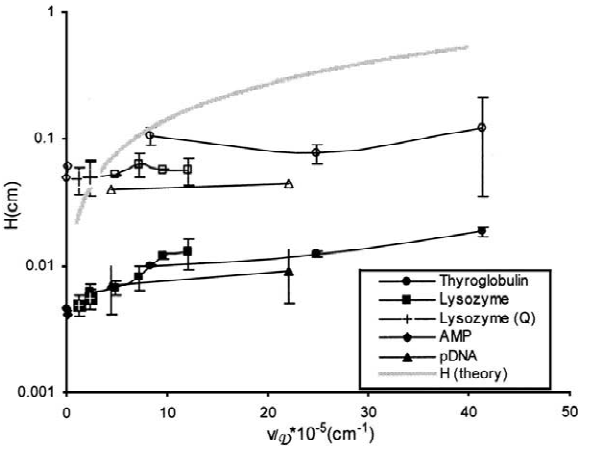

Fig. 4. Plate height vs. scaled velocity for all forward-flow (open symbols) and reverse-flow (closed symbols) dispersion tests using the 10-ml Mustang-Q and -S [12]. For comparison, the plate heights for an ideal bed packed with 15 μm particles were predicted using Eq. (5).

membranes have short mass transfer distances and are able to remain efficient with even very large biomolecules. The forward-flow plate heights, representative of the actual performance of both 10-ml Mustang modules, are comparable to the packed-bed plate heights at low velocities and show negligible increases at high velocities. The macroscopic flow is a significant source of dispersion, with tailing causing the forward-flow plate heights to be an order of magnitude greater than the respective reverse-flow plate heights.

4.2. Plasmid adsorption

Batch adsorption data were measured for the 6.1-kb plasmid adsorbing to sheets of the Mustang-Q membrane at various ionic strengths following the procedure described above. The results plotted in Fig. 5 show the solid-phase plasmid concentration against liquid phase plasmid concentration at NaCl concentrations ranging from 100 to 1000 m*M*. Note that the solid-phase concentration is reported as mass per cross-sectional area of the membrane sheet, not per surface area within the membrane sheet. Adsorption strength decreased with increasing ionic strength, and no adsorption was observed at 1000 m*M* NaCl. The data were fit to the Langmuir isotherm, yielding an estimated capacity q_{max} of just under 100 $\mu g/cm^2$. Given the cross-sectional area (~12 cm^2) and number of membrane sheets (~90) stacked in the 10-ml Mustang-Q, the plasmid capacity for the stacked membrane unit is calculated as 10 mg/ml. This is a factor of two greater than the greatest plasmid capacity reported for ''superporous'' particles, and five times greater than the capacity reported for 15 μm particles [6].

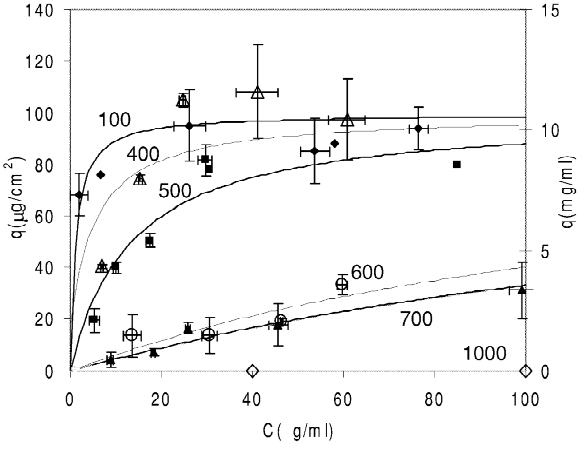

Fig. 5. Adsorption isotherms for adsorption of 6.1-kb plasmid DNA to anion-exchange membranes. Experimental data (points) and fitted isotherms (lines) are for plasmid binding at 100 (●), 400 (△), 500 (■), 600 (○), 700 (▲), and 1000 (◊) m*M* NaCl.

Table 2
Dissociation constants for plasmid DNA at various salt concentrations

Salt concentration (m*M* NaCl)	K_D (μg/ml)
100	1.2
400	4.7
500	13.3
600	148
700	202

The desorption constant, K_D in Eq. (11), was estimated at each loading salt concentration using a non-linear fit. As listed in Table 2, the desorption constants are very small for equilibration at salt concentrations of 500 m*M* and smaller. This is highly favorable for the capture of plasmid DNA from dilute solutions, as K_D is equal to the liquid-phase plasmid concentration in equilibrium with one-half the maximum binding capacity. Loading solutions with plasmid concentrations greater than K_D utilizes the large capacity of the ion-exchange membranes.

5. Conclusions

In this study, anion-exchange membranes were characterized for their utility in purification of very large biomolecules such as plasmid DNA. Most important is the large capacity of membranes for plasmid DNA as compared to conventional porous adsorbents. The measured capacity of 10 mg/ml is significantly larger than particulate adsorbents that have capacities limited by small pores. Furthermore, membrane efficiencies remain very high for large biomolecules that have diffusion coefficients orders of magnitude less than a small protein, confirming the absence of mass transfer limitations. The intrinsic membrane plate heights are over an order of mag-

nitude less than plate heights predicted for bed packed with 15 μm particles. The differences in plate heights are most pronounced at high values of v/D, where mass transfer limitations are most significant in porous particles.

Advantages of adsorptive membranes for purification of large biomolecules may be summarized as follows: porous beads limited by surface binding may see capacity improvements by decreasing the particle diameter, which comes at the expense of very large pressure drops, or by increasing the pore size, which leads to significant mass transfer limitations as the large biomolecules must diffuse through stagnant fluid. Adsorptive membranes do not have such trade-offs, as the large convective through-pores are accessible to large biomolecules, diffusional limitations are minimal, and the high porosity, large cross-sectional area, and minimal thickness allow for operation at low pressure drops.

References

[1] G.N.M. Ferreira, G.A. Monteiro, D.M.F. Prazeres, J.M.S. Cabral, Trends Biotechnol. 18 (2000) 380.
[2] N.A. Horn, J.A. Meek, G. Budahazi, M. Marquet, Hum. Gene Ther. 6 (1995) 565.
[3] D.M.F. Prazeres, T. Schluep, C. Cooney, J. Chromatogr. A 806 (1998) 31.
[4] D.W. Kahn, M.D. Butler, D.L. Cohen, M. Gordon, J.W. Kahn, M.E. Winkler, Biotechnol. Bioeng. 69 (2000) 101.
[5] G.N.M. Ferreira, J.M.S. Cabral, D.M.F. Prazeres, Biotechnol. Prog. 16 (2000) 416.
[6] M.S. Levy, R.D. O'Kennedy, P. Ayazi-Shamlou, P. Dunnill, Trends Biotechnol. 18 (2000) 296.
[7] A. Ljunglof, P. Bergvall, R. Bhikhabhai, R. Hjorth, J. Chromatogr. A 844 (1999) 129.
[8] S. Yamamoto, E. Miyagawa, J. Chromatogr. A 852 (1999) 25.
[9] C.G. Huber, J. Chromatogr. A 806 (1998) 3.
[10] A. Strancar, A. Podgornik, M. Barut, R. Necina, Adv. Biochem. Eng./Biotechnol. 76 (2002) 49.
[11] H.W. Yang, C. Viera, J. Fischer, M.R. Etzel, Ind. Eng. Chem. Res. 41 (2002) 1597.
[12] M.A. Teeters, T.W. Root, E.N. Lightfoot, J. Chromatogr. A 944 (2002) 129.
[13] C. Charcosset, J. Chem. Technol. Biotechnol. 71 (1998) 95.
[14] J. Thommes, M.R. Kula, Biotechnol. Prog. 11 (1995) 357.
[15] D.K. Roper, E.N. Lightfoot, J. Chromatogr. A 702 (1995) 3.
[16] M.S. Jeansonne, J.P. Foley, J. Chromatogr. 594 (1992) 1.
[17] P. Schneider, J.M. Smith, AIChE J. 14 (1968) 762.
[18] A.M. Athalye, S.J. Gibbs, E.N. Lightfoot, J. Chromatogr. 589 (1992) 71.
[19] R.B. Bird, W.E. Stewart, E.N. Lightfoot, Transport Phenomena, Wiley, New York, 1960.
[20] T. Farkas, G.M. Zhong, G. Guiochon, J. Chromatogr. A 849 (1999) 35.
[21] D.K. Roper, E.N. Lightfoot, J. Chromatogr. A 702 (1995) 69.
[22] M. Kaminski, J. Chromatogr. 589 (1992) 61.
[23] J. Moscariello, G. Purdom, J. Coffman, T.W. Root, E.N. Lightfoot, J. Chromatogr. A 908 (2001) 131.
[24] D.E. Smith, T.T. Perkins, S. Chu, Macromolecules 29 (1996) 1372.
[25] C. Tanford, Physical Chemistry of Macromolecules, Wiley, New York, 1966.